Tracking and Fusion in Multistatic Sensor Networks[1]

Murat Efe
Ankara University
Faculty of Engineering
Electrical and Electronics Eng. Dept.
06100, Tandogan - Ankara
TURKEY

efe@eng.ankara.edu.tr

ABSTRACT

In this study some practical aspects of working with multistatic sensor networks are addressed. Firstly the amount of information available through multistatic configuration is analyzed with respect to the number of transmitter/receiver pairs as well as the geometry. Then an example of multitarget tracking in a multisensory network is given where the association of measurements to targets is done through assignment. Lastly the use of an effective statistical tool, namely, observed information matrix, in multistatic tracking and fusion is discussed.

1.0 INTRODUCTION

A multistatic radar network contains multiple spatially diverse transmitters and receivers where each transmitter receiver pair forms a bistatic radar. In other words, multistatic radar network can be thought as a system where several bistatic radars are deployed to communicate with each other and share their information gathered from the environment for detecting and tracking targets. Bistatic radar systems [1] differ from the typical modern active radar systems through consisting of spatially diverse transmitter and receiver sites. In these systems, surveillance region is illuminated by the signal transmitted from the transmitter site and receiver antennas listen the signals scattered form the targets present in that region. Target detection and the extraction of the available measurements are carried out at the receiver site via proper signal processing techniques. Although bistatic radar systems have been of interest to researchers since the early days of radar, it is quoted in [2] that the interest in bistatic radar gets renewed approximately every fifteen years. Recently, there has been a new surge of interest in the studies on bistatic radar systems. The promise of cheap and quiet receivers, aspect angle diversity and improved target tracking accuracy could be considered as the main motivators for this resurge of interest [1].

Bistatic radars generally have the capability of measuring bistatic ranges and range rates of the targets. In addition to these measurements, it is possible to measure azimuth and elevation angles of the targets with respect to the receiver. However, measuring angle requires more complex antennas and signal processing algorithms to be implemented at the receiver site. The measurements obtained from a bistatic radar (with or without angle measurements) are highly nonlinear in nature. Therefore, target tracking using bistatic radar measurements is a nonlinear state estimation problem in nature and several algorithms addressing this problem can be found in the literature. The most commonly known algorithm proposed for the nonlinear state estimation is the *Extended Kalman Filter,* (EKF) [3] in which nonlinear functions are linearized via Taylor series expansion. Another way of dealing with the nonlinearity in state estimation is employing *Unscented Kalman Filter* (UKF) [4] in which statistical linearization is performed via unscented transform rather than the analytical linearization as in EKF. UKF resembles the Monte Carlo integration type methods, however, there is a fundamental difference on generating sample points step of the UKF in which the samples are drawn in a non-random fashion. Monte Carlo integration type methods also produce a solution

1 Results presented in this study were obtained through joint works with Ali Onder Bozdogan, Gokhan Soysal and Roy Streit. Their cooperation is greatly appreciated.

to the nonlinear state estimation problem. Monte Carlo integration based particle filters [5] have drawn interest for the solution of the nonlinear state estimation problem due to the advances of the computational power in recent years.

In a multistatic radar system, there are more than one bistatic radar (sensor) which means, the number of possible information sources from the environment can be greater than one at a time. Therefore, the information gathered from the different sensors should somehow be combined. This situation is no different than the monostatic sensor network case and could be addressed via utilizing either centralized or distributed data fusion techniques. Centralized data fusion is based on collecting all available information (measurements) from the sensors at the fusion center and combining the information using proper algorithms. This technique requires communication links between sensors and the fusion center which causes huge communication overheads. Moreover, centralized data fusion is not robust as all data fusion process is carried out at single station. On the contrary, distributed data fusion is a more robust technique where data fusion is carried out at each sensor by combining the information gathered from the neighboring sensors (the sensor group connected to each other). In this technique, each sensor has its own state estimator and is capable of combining the information (measurements or state estimations obtained at the other sensors) acquired from the other sensors.

In this study we are mainly interested in the amount of information available in a multistatic sensor network, how it varies with respect to the transmitter/receiver geometry and how we can make use of available information in tracking and fusion applications in these networks. We will start with the analysis of information change in the multistatic network, then apply an assignment based association and tracking for a multiple target application using measurements provided by a multistatic network. Then we will conclude by showing an alternative way of representing the information and utilizing it in tracking and fusion application.

2.0 INFORMATION ANALYSIS IN A MULTISATIC NETWORK

Performance of any tracker is affected by target detection process by means of durability of detection in time and accuracy of the obtained measurements. While, detecting a target in every scan guaranties to have information about the target state, accuracy of the observed measurements will determine the accuracy of the estimated target state that can be achieved by the tracking algorithm. Accuracy of the measurements can be thought as the amount of information about target state and can be modeled through the use of Fisher information [3]. In this view, in a passive radar network the amount of information contained in target originated measurement about target state would depend on the number of transmitter–receiver pairs (which we will call a `sensor`), locations of the pairs and the target state. In this study the relation between detection and tracking in passive networks has been used to determine the effect of number of sensors and sensor geometry on the information gathered from the target originated measurement through the analysis of Fisher Information Matrix (FIM). Variation of available information depending on number/geometry of sensors and target states can be monitored by observing the FIM. Diagonal elements of the inverse of FIM are the lowest achievable variances of the parameters to be estimated, square root of which can be defined as the uncertainty pertaining to these parameters. The obtained uncertainty, then, can be utilized to define a bound for achievable accuracy of estimated target state in passive radar networks.

In this part of the study, an analytical study, based on the FIM, regarding the performance of passive radar networks is presented. We aim to present the performance limits with respect to varying sensor numbers and geometry. For this purpose, a single transmitter multi receiver passive radar network with the capability of measuring bistatic range and range rate has been modeled and Fisher information has been computed independent of target detection and tracking processes where the target was assumed to be moving on a grid defined in 3D Cartesian space. FIMs have been computed based on static parameter estimation at every possible location of the target for different configurations (different number of sensors and different sensor geometry) in a multistatic radar network.

2.1 Likelihood Function and the Fisher Information Matrix

Assume that θ is the vector valued parameter that contains positions x, y, z and velocities vx, vy, vz in 3D Cartesian space to be estimated. L_r and L_t are locations of the receiver and transmitter respectively.

$$\theta = [x \quad vx \quad y \quad vy \quad z \quad vz]^T \tag{1}$$

$$L_r = [x_r \quad y_r \quad z_r]^T \tag{2}$$

$$L_t = [x_t \quad y_t \quad z_t]^T \tag{3}$$

Let R_r and R_t denote the distances between the receiver and the target of interest and between the transmitter and target of interest respectively. Assume that range rate of the target with respect to the receiver and transmitter are $\dot{R}_r$ and $\dot{R}_t$ respectively. Then, one can write bistatic range and range rate measurements generated by a transmitter–receiver pair as

$$r = R_r + R_t + \varepsilon_r \tag{4}$$

$$\dot{r} = \dot{R}_r + \dot{R}_t + \varepsilon_{\dot{r}} \tag{5}$$

where

$$R_r = \sqrt{(x - x_r)^2 + (y - y_r)^2 + (z - z_r)^2} \tag{6}$$

$$R_t = \sqrt{(x - x_t)^2 + (y - y_t)^2 + (z - z_t)^2} \tag{7}$$

$$\dot{R}_r = \frac{(x - x_r)vx + (y - y_r)vy + (z - z_r)vz}{R_r} \tag{8}$$

$$\dot{R}_t = \frac{(x - x_t)vx + (y - y_t)vy + (z - z_t)vz}{R_t} \tag{9}$$

Here ε_r and $\varepsilon_{\dot{r}}$ are measurement errors which are assumed to be mutually independent Gaussian processes with zero mean and variances σ_m^2 and $\sigma_{\dot{m}}^2$ respectively. Assuming that that σ_m^2 and $\sigma_{\dot{m}}^2$ are known, then the likelihood function of the parameter θ can be written as

$$\Lambda(r, \dot{r} \mid \theta, \sigma_m, \sigma_{\dot{m}}) = \frac{1}{\sqrt{2\pi}\sigma_m} \exp\left(\frac{-(R_r + R_t - r)^2}{2\sigma_m^2}\right) \frac{1}{\sqrt{2\pi}\sigma_{\dot{m}}} \exp\left(\frac{-(\dot{R}_r + \dot{R}_t - \dot{r})^2}{2\sigma_{\dot{m}}^2}\right) \tag{10}$$

In the presence of more than one transmitter-receiver pairs the likelihood function can be defined as the multiplication of the individual likelihood functions of each pair under the assumption that measurement errors are mutually independent, as given by Eq. (11)

$$\Lambda(Z \mid \theta, Z_\sigma) = \prod_{i=1}^{k} \Lambda(r_i, \dot{r}_i \mid \theta, \sigma_{m_i}, \sigma_{\dot{m}_i}) \tag{11}$$

In Eq. (11), Z is set of measurements acquired from the sensors at time t and Z_σ is set of standard deviations pertaining to the measurements. For the described system the Fisher information matrix is defined as,

$$FIM = -E\left[\nabla_\theta \nabla_\theta^t \ln(\Lambda(\theta))\right]_{\theta=\theta_0} \tag{12}$$

where ∇_θ is the gradient operator. Logarithm of the likelihood function for a single transmitter-receiver pair is

$$\varphi = \ln(\Lambda(\theta)) = -\frac{(R_r + R_t - r)^2}{2\sigma_m^2} - \frac{(\dot{R}_r + \dot{R}_t - \dot{r})^2}{2\sigma_{\dot{m}}^2} - \ln(2\pi\sigma_m\sigma_{\dot{m}}) \tag{13}$$

then the Fisher information matrix is written as

$$FIM = -E\begin{bmatrix} \frac{\partial^2\varphi}{\partial x^2} & \cdots & \frac{\partial^2\varphi}{\partial x \partial v_z} \\ \vdots & \ddots & \vdots \\ \frac{\partial^2\varphi}{\partial v_z \partial x} & \cdots & \frac{\partial^2\varphi}{\partial v_z^2} \end{bmatrix} \tag{14}$$

Derivation of the elements of FIM is given in the Appendix for a single sensor. However, it can be easily expanded to multiple sensor case by using Eq. (11) as sum of FIMs.

2.2 Transmitter/Receiver Configuration

In the setup, the illuminator is placed at the origin of the coordinate system. Encircling the illuminator are the six receivers located at the vertices of a hexagon centered at the origin and the target is assumed to be moving on a grid defined in 3D Cartesian space as illustrated in Figures 1a and 1b. Also it is assumed that target is moving at constant altitude of 5 km and is stationary at the grid point during the measurement extraction process.

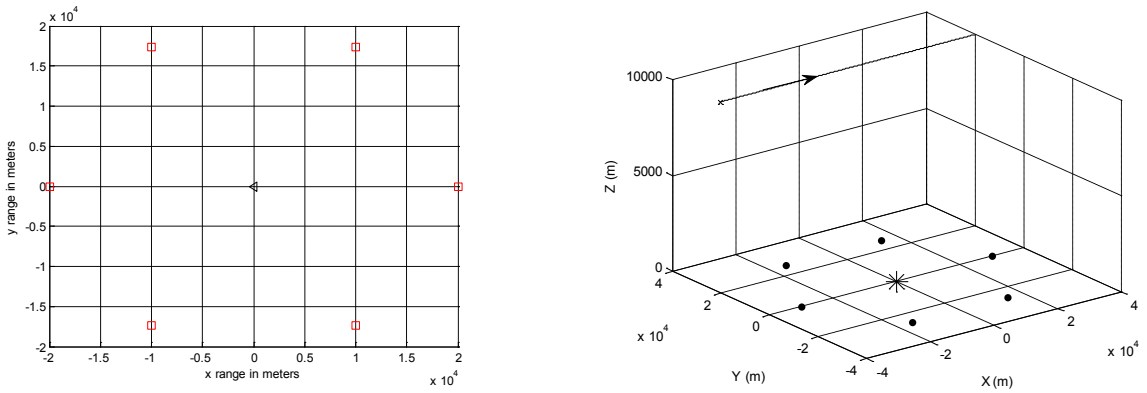

(a) (b)

Figure 1: (a) Transmitter (black triangle), receiver (red square) locations (b) target trajectory

It is assumed that, in this single transmitter multi receiver multistatic radar network, each transmitter-receiver pair produces bistatic range and range rate which are corrupted by additive white Gaussian noise with known mean and variance. In the analysis, plane earth model is used and coverage area of the passive radar network is kept limited in both X and Y axes in the interval of (-200km, 200km). It was assumed that target is moving

in a 400 m long discrete grid in both X and Y axes and target movement is assumed independent between two locations. Target was assumed to be moving in 3D Cartesian space according to state vector $[x\ \dot{x}\ y\ \dot{y}\ z\ \dot{z}]^T$ at a fixed altitude. Measurements obtained from each transmitter-receiver pair for 3D target state have been given as

$$R = \sqrt{(x-x_r)^2+(y-y_r)^2+(z-z_r)^2} + \sqrt{(x-x_t)^2+(y-y_t)^2+(z-z_t)^2} + \varepsilon_r \tag{15}$$

$$\dot{R} = \frac{(x-x_r)\dot{x}+(y-y_r)\dot{y}+(z-z_r)\dot{z}}{\sqrt{(x-x_r)^2+(y-y_r)^2+(z-z_r)^2}} + \frac{(x-x_t)\dot{x}+(y-y_t)\dot{y}+(z-z_t)\dot{z}}{\sqrt{(x-x_t)^2+(y-y_t)^2+(z-z_t)^2}} + \varepsilon_{\dot{r}} \tag{16}$$

In Eqs. (15) and (16), subscripts "r" and "t" indicate the location of receiver and transmitter in 3D Cartesian space respectively. Additive error terms ε_r and $\varepsilon_{\dot{r}}$ are modeled as white Gaussian processes with zero mean and variances of $10000\,m^2$ and $1(m/\sec)^2$ respectively.

The single transmitter multi receiver configuration is modeled in two principal configurations of transmitter-receiver locations. Receivers are placed to form a symmetrical constellation (hexagon or circle). Two different transmitter locations are assumed in the circular receiver configuration of which one is at the center of receiver circle and the other is out of it. Thus, having a transmitter in a controlled territory and a transmitter which is located out of the homeland borders are modeled. In the second configuration the transmitter is located at 75 km from the center of receiver circle and at 45° azimuth angle measured counterclockwise from the X axis measured. After fixed transmitter locations are determined, several different transmitter-receiver geometries are generated by changing the number of receivers and the radius of the receiver circle. The number of receivers has been changed from 3 to 72 which corresponds to 120° separation between adjacent receivers in the 3 receiver case and 5° separation between adjacent receivers in the 72 receiver case. For the first configuration, the smallest radius of the receiver circle is set to 10 km and it is increased to 100 km by 5 km increments. Radius of the receiver circle is also varied between 10-50 km with 5 km increments for the configuration in which transmitter was located outside the circle. For all configurations, altitude of receivers and transmitters was assumed to be same and set to the ground level.

Variation of the Fisher information, i.e. changes in uncertainty, w.r.t. the target state and transmitter-receiver configuration have been analyzed in terms of Total Position Uncertainty (TPU), Total Velocity Uncertainty (TVU) and Normalized Coverage Area (NCA) through simulations. TPU and TVU are computed for the kth position of the target on the grid as follows,

$$U_k = \sqrt{diag(FIM_k^{-1})} = \left[\Sigma_{xx}^k\ \Sigma_{\dot{x}\dot{x}}^k\ \Sigma_{yy}^k\ \Sigma_{\dot{y}\dot{y}}^k\ \Sigma_{zz}^k\ \Sigma_{\dot{z}\dot{z}}^k\right] \tag{17}$$

$$P_k = \Sigma_{xx}^k + \Sigma_{yy}^k + \Sigma_{zz}^k \tag{18}$$

$$V_k = \Sigma_{\dot{x}\dot{x}}^k + \Sigma_{\dot{y}\dot{y}}^k + \Sigma_{\dot{z}\dot{z}}^k \tag{19}$$

$$TPU = \frac{1}{N}\sum_{k=1}^{N} P_k \tag{20}$$

$$TVU = \frac{1}{N}\sum_{k=1}^{N} V_k \tag{21}$$

where FIM_k and "$diag$" indicate Fisher information matrix at the kth position and the diagonal elements respectively. However, not all target positions (cells of grid) contribute to summations defined by Eqs. (20) and (21). Only the cells for which the computed uncertainty value is less than 300 m in position and 4 m/sec in velocity for all axes have been taken into account. Thus, zones where position and velocity of the target can be estimated with significant error level are determined. NCA was determined as the ratio of area of cells which have significant uncertainty levels as defined above to area of receiver circle as given by Eq. (22)

$$NCA = \frac{N 2\pi r_c^2}{2\pi r^2} = \frac{N r_c^2}{r^2} \tag{22}$$

where, r, r_c, N are radius of the receiver circle, radius of a cell and the number of significant cells respectively.

2.3 Simulation Results for Information Analysis

For the first configuration where the transmitter is located at the center, variation of TPU and TVU with respect to the change in the number of receivers and radius of receiver circle are shown in Figs. 2a and 2b. Total uncertainties in position and velocity reduce exponentially with the increasing number of receivers for all radiuses. This is expected due to the fact that, increase on amount of information by deploying more transmitter-receiver pairs and gathering more measurements leads to more accurate state estimation. However, it is seen explicitly in the Figures that while changing the number of receivers from 3 to 10 provides significant improvement in uncertainty, contribution from the addition of a new receiver reduces rapidly after the 10th receiver. This outcome is supported by the NCA analysis which is presented in Fig. 3a in which a rapid growth in NCA is seen with increasing the number of sensors from 3 to 10 whereas the growth rate decreases for each sensor added after the 10th.

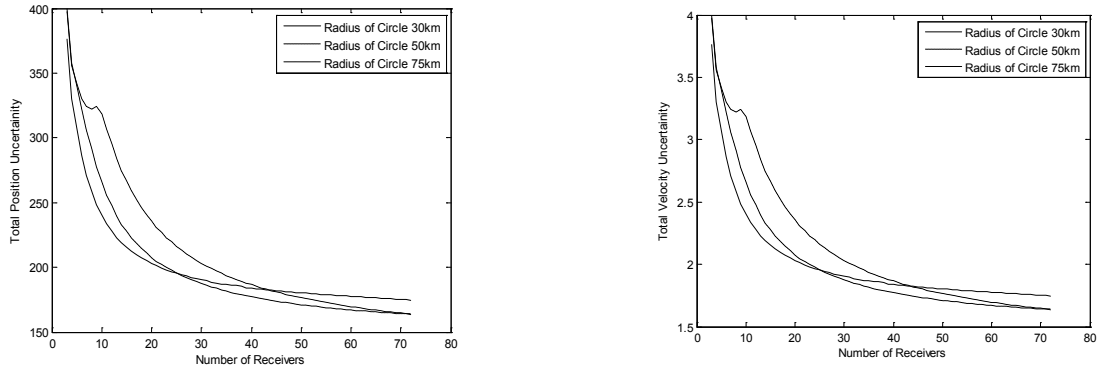

(a) (b)

Figure 2: Variation of uncertainty with respect to the number of receivers (a) position (b) velocity

Another result worth mentioning is the effect of radius of the receiver circle. Smaller radius achieves bigger NCA in comparison to the larger receiver circle. For instance the NCA has been 2.5 times the area of the receiver circle with the 30 km receiver circle when the maximum numbers of receivers is deployed. 100% coverage of the region bounded by receiver circle could be achieved by exploiting 6, 8 and 15 receivers for 30km, 50km and 75km receiver radius respectively.

Analysis of TPU, TVU and NCA has shown that growth in the number of transmitter-receiver pairs deployed in a passive radar network has the advantage of collecting more information from the target of

interest, i.e. estimating target state more accurately and covering a greater region. However in real world implementations, utilizing a big number of transmitter-receiver pairs increases the communication cost and the measurement to track data association problem becomes almost unsolvable in real time. Therefore, a feasible passive radar system should be designed to have the appropriate number of sensors to cover the region of interest with acceptable accuracy while allowing computations to be carried out in real time. Such a system can be designed by utilizing the results presented in Figs.2a, 2b and 3a. As mentioned previously 100% coverage of the region of interest with uncertainties in position and velocity less than 300 m and 4 m/sec respectively can be achieved by exploiting 6 receivers located on a circle with radius 30 km. For further analysis, detailed simulation results have been obtained for the 6 receiver configuration. First of all, bounds of the NCA have been investigated by expanding the radius of the receiver circle in 10 km, 100 km interval with 5km increments and the results are given in Fig. 3b.

As shown in Fig. 3b, the NCA is greater than 1, i.e. bigger than the area of the receiver circle, while the radius of the circle varies between 10 km and 37 km. The coverage, then, decreases to 20% beyond 37 km radius for the fixed number of receivers. The NCA is approximately 1.25 when the radius is 30km which is a fine coverage and image of this region has been given in Fig. 4. The region depicted in Figure 4 may be thought as the tracking zone where the upper bound of tracking error is 300 m in position and 4 m/sec in velocity around the edges of the region.

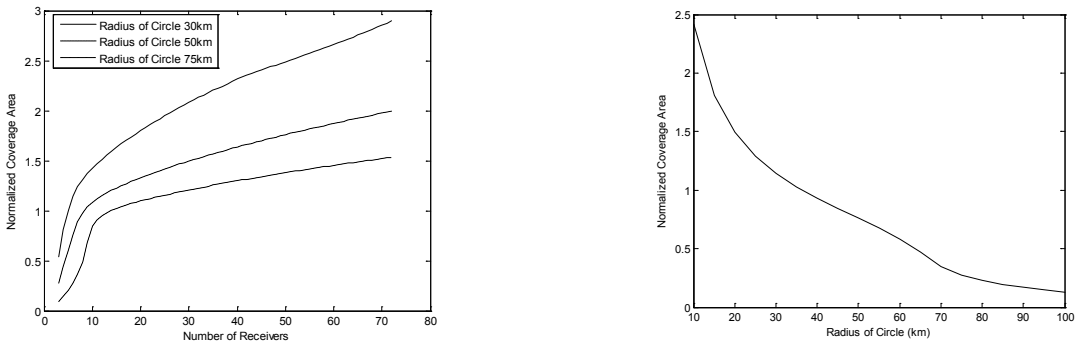

(a) (b)

Figure 3: Variation in the normalized coverage area (a) w.r.t. number of receivers (b) w.r.t. radius of the receiver circle

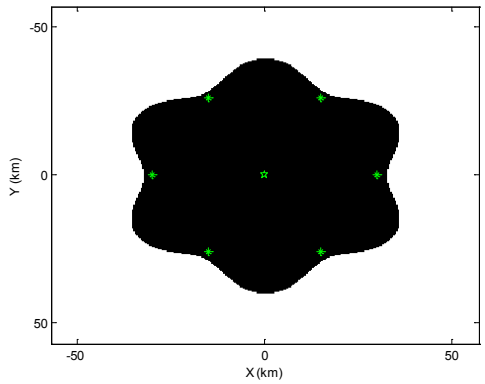

Figure 4: Computed tracking zone where position uncertainty is less than 300 m and velocity uncertainty is less than 4 m/sec

Distribution of position uncertainties within the tracking zone has been given for X, Y and Z axes in Figs. 5a, 5b and 5c respectively. While uncertainties on X and Y axes vary in the interval of 30-80 m, the uncertainty on Z axis varies in a wider range (30-300m) and these results show that bounds of the tracking zone are determined by the uncertainty on Z axis. Similar distribution patterns and higher uncertainty level on Z axis have been obtained for velocity uncertainties and results are given in Figs. 6a, 6b and 6c.

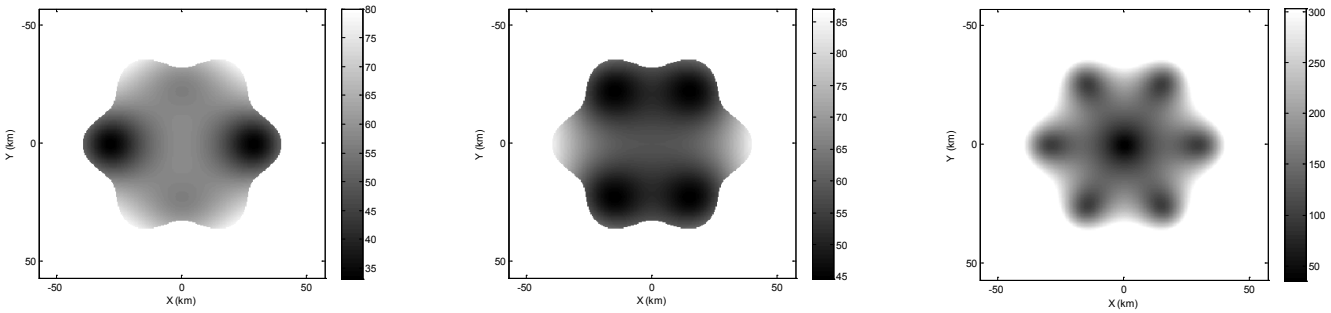

(a) (b) (c)

Figure 5: Distribution of position uncertainty on (a) X, (b) Y, (c) Z

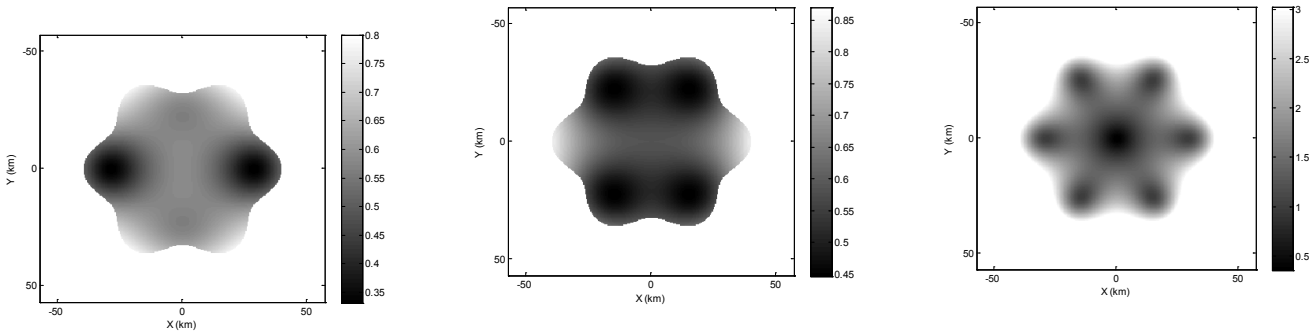

(a) (b) (c)

Figure 6: Distribution of velocity uncertainty on (a) X, (b) Y, (c) Z

Simulation results for the configuration in which transmitter is located outside the receiver circle have shown that, the change in the location of transmitter has a great effect on the size of the coverage region as well as uncertainty levels. Coverage region of a passive radar network comprising 6 receivers located on a circle with radius 30 km is shown in Fig. 7a and as it is seen from the figure, the region lying between the transmitter and center of the circle could not be covered by the passive radar network. In order to cover this region, one can locate another transmitter at 225° measured CCW from the X axis that results in 12 transmitter-receiver pairs. However, this is not feasible under the assumption that emission sources are "illuminators of opportunity" and they are not under control. Another solution to this problem would be to increase the number of receivers until region bounded by the receiver circle is fully covered. Adequate number of receivers has been found to be 10 where the coverage area for this configuration is depicted in Fig. 7b. Further analysis has been carried out in order to determine the achievable maximum radius of the receiver circle for the 10 receiver configuration. Circle radius has been expanded from 30 km to 50 km by 1 km increment and variation of the covered region observed. Simulations have revealed that the achievable maximum radius for this configuration is 40 km beyond which a circular gap occurs due to higher uncertainties in position and velocity as depicted in Fig. 7c.

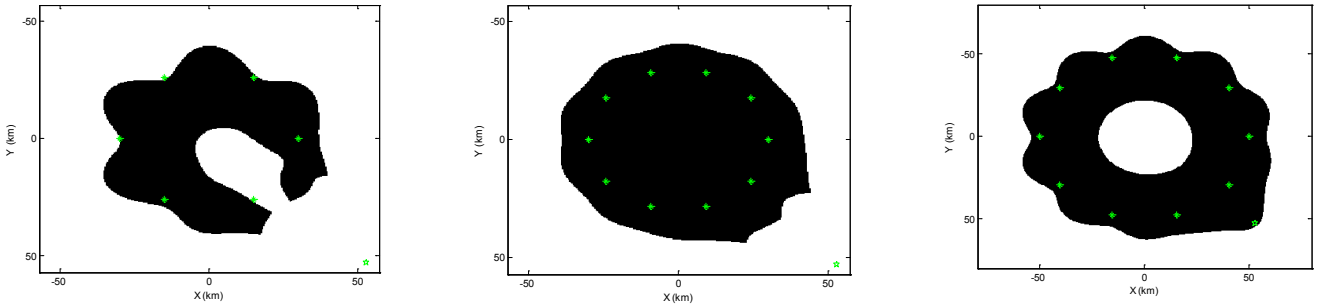

(a) (b) (c)

Figure 7: Computed tracking zone (a) 6 receivers, (b) 10 receivers, (c) beyond the achievable maximum receiver circle radius

Moreover, variations of position and velocity uncertainties with respect to the number of receivers for the transmitter outside the receiver circle case are given in Figs. 8a and 8b respectively. These results were obtained for case where radius of receiver circle is 30 km.

If one made a comparison between the position uncertainties obtained by configurations one and two, it would be seen that there is approximately 100 m difference in position uncertainties for the two configurations whilst second configuration deploys more receivers than first one. Similar results are obtained for the velocity uncertainty as well. Although the simulation results presented here depict a circular sensor geometry, similar results would be obtained for any symmetrical sensor geometry where the minimum number of sensors should be 6, i.e., hexagon, octagon etc.

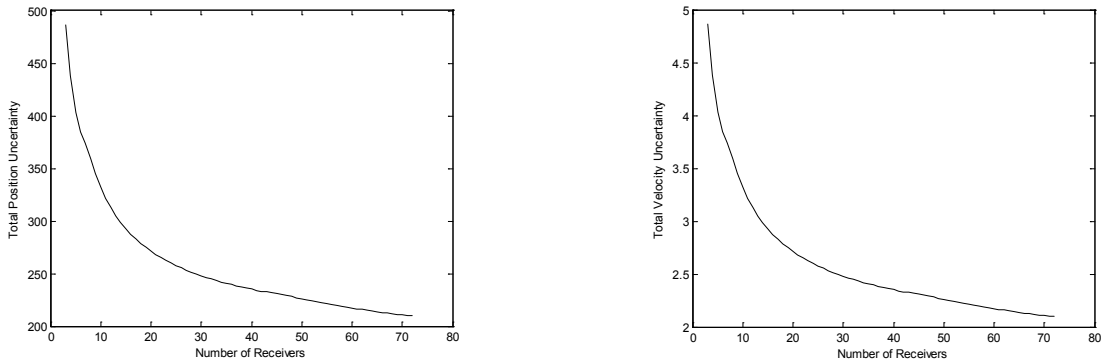

(a) (b)

Figure 8: transmitter outside the receiver circle case (a) variation of position uncertainty (b) variation of velocity uncertainty

3.0 MULTISTATIC TRACKING

In this part of the study, passive bistatic radar systems (PBR) that use non-radar transmitters (*transmitters of opportunity)* as their illumination source are considered. PBR systems described in the open literature generally utilize cheap antenna arrays that provide poor angular resolution. The main observables for such systems are the bistatic range and bistatic range rate of the target of interest. Therefore, using any such system, multilateration is necessary in order to estimate a target's position. However, considering a realistic

multitarget tracking scenario, multilateration posits a hard data association problem. Nevertheless, the open literature on PBR systems is generally oriented towards the issues of detection while neglecting tracking. There is only few published research that directly address the issue of fusing multiple sets of measurements from separate bistatic receiver-transmitter pairs. The pioneering work on the subject [6] addressed the issue of deriving a unique tracking algorithm structure for multistatic radar systems for single target tracking without considering any specific transmission source. The study also assumed that the angle measurement is available along with the range measurement. In [7] the authors used probability hypothesis density (PHD) filter in a 2D tracking scenario for a passive multistatic radar system (PMR) that utilize multiple FM transmitters and a single receiver. In this contribution, our interest lies mainly in 3D tracking. Although conceptually extendable to the three dimension case, the performance of the PHD filter in such a scenario can be a case for a further study. In [8] a multi hypothesis filters (MHT) based multistage tracker was used to track a single target in clutter. The MHT algorithm suggested in [8] utilized first a 1D range tracker to suppress clutter measurements, then 1D range tracks were fused to find likely 2D Cartesian target estimates. Finally, likely 2D Cartesian target estimates were fused to get full 3D tracks. The suggested multistage structure of the tracking algorithm was designed to reduce the measurement to target association load. However, as for the detection ranges considered, the number of possible targets might overload even a multistage tracker. Furthermore, for targets that are close to the receiver, the 2D location estimates formed using an expected target height could vary depending on the true target height; thus reducing the 2D to 3D information flow.

In this study we consider a relatively difficult multitarget tracking in clutter problem with a multistatic radar system where crossing targets and targets flying in formation are present. Such a scenario requires the multidimensional assignment problem to be solved. We implement a tracking algorithm to be used with a network of six bistatic receivers observing a hexagonal region. One primary difference of our approach from the first two studies given above is that our radar system is composed of multiple receivers listening to a single transmitter as opposed to a single receiver listening to multiple transmitters. While increasing the receiver cost and requiring synchronization and communication between receivers and a data processing center, this cellular type approach provides spatial separation for distant targets (targets in different cells), thus reducing number of association hypotheses that the assignment problem needs to solve.

The tracker presented in this study is based on multidimensional assignment algorithm [9], [10]. Similar to [10], at each scan tracks are associated with a set of measurements that minimize the global track to measurement association cost. Unassociated measurements are then fed to the track initiator module to test for new tracks. It is assumed that probability of detection is high so that at least three measurements are received from each target in the surveillance region, thereby enabling 3D tracking.

3.1 Transmitter/Receiver Geometry

In the tracking setup, the configuration depicted in Fig. 1 is used in which, the illuminator is placed at the origin of the coordinate system. Encircling the illuminator are the six receivers located at the vertices of a hexagon centered at the origin. The side length of the hexagon is taken to be 20 kilometers.

Although the given specific transmitter-receiver geometry has been assumed, the study, with ease, can be extended to the cases where transmitter is located anywhere in the region encircled by the receivers or even where the transmitter is located outside the receiver formation. The location of the transmitter will affect the amount of information contained in an observation that a receiver-transmitter pair has produced [11]. This will in return affect the tracker's performance. However, the design of the multidimensional assignment tracker is independent of the receiver-transmitter geometry.

3.2 Measurement Model

Each receiver measures bistatic range and bistatic range rate of a target corrupted by additive white Gaussian noise. Given the state of a target *X* at time *t* to be defined by a vector consisting of the target's position and velocity values as shown in Eq. (23), the bistatic measurement of target's range and range rate for a receiver *k* located at R_k can be found by using Eq. (2-3) [3]

$$X[t] = [x\ \dot{x}\ y\ \dot{y}\ z\ \dot{z}]^T \tag{23}$$

$$r_k = \|p\| + \|p - R_k\| + \varepsilon \tag{24}$$

$$\dot{r}_k = [\frac{p}{\|p\|} + \frac{p - R_k}{\|p - R_k\|}]^T . v + \xi \tag{25}$$

In Eqs. (24) and (25), p denotes the position and v denotes the velocity vector of the target X. ε and ξ are measurement noises for range and range rate respectively. It is assumed that receivers in the constellation report their measurements to a data processing center synchronously and registration errors are not modeled.

3.3 Tracking Algorithm

The tracking algorithm implemented in this study comprises two main modules, namely the tracker and the track initiator. In the design of the tracking algorithm, it is assumed that measurements collected from each receiver are reported to a data processing center periodically. Furthermore, communication with receivers is assumed to be synchronized.

At the data processing center, received measurements from each time scan are first populated and collected in a measurement list. The measurement list is then presented to a list of confirmed tracks and generic validation gating [9] is applied to determine likely track-measurement combinations. Each measurement combination[2] that has passed the ellipsoidal validation gating is filtered with the state estimator and its *track score* is calculated. The multidimensional assignment algorithm is next applied to determine the track-measurement combinations that optimize the global track score. The track list is then updated with the optimal association and the associated measurements are dropped from the measurements list. For the tracks that are not associated with a valid measurement set, a track drop iterator is incremented. If the track drop iterator is incremented for four consecutive scans, then the track is dropped. This completes the operation of the tracker module.

The remaining measurements that have not been associated with any of the confirmed tracks are later collected in the unassociated measurement list, whose elements are fed to the track initiator module. At the track initiator module, the unassociated measurement list is firstly presented to a list of tentative tracks [10] and the tracker module is called back to determine tentative track – measurement associations. The tentative tracks that are updated with a valid set of measurements are then appended to the tracks list and their associated measurements are dropped from the measurements list. The unassociated tentative tracks are dropped from the tentative tracks list.

The final measurement list is used to initiate new tentative tracks. In order to reduce the number of optimizations performed in this step, every measurement that will go through further processing is required to have at least one related measurement (range only validation gating) from the previous two scans[3] . Maximum likelihood estimates of hypothesized target states using combinations of range only validation gated measurements from each receiver are then computed. In order to further reduce the number of

2 A valid set of measurements constitutes at least 3 detections. When the detection probability of each receiver is taken to be 0.9 and independent detection among receivers is assumed, a target produces at least 3 detections with a probability of 0.9987.

3 The range only validation gating is applied to a copy of full sets of measurements where the associated measurements are not dropped.

optimizations, each target state estimate is required to have at least four detections[4]. A track score is calculated for each hypothesized target and the multidimensional assignment algorithm is used to extract tentative tracks as shown in [9]. This step completes the operation of the track initiator module.

3.3.1 Target Motion Model

The target state is assumed to evolve according to the discrete white noise acceleration model (DWNA) [3]. The acceleration in each coordinate is assumed to be normally distributed with zero mean and independent from the accelerations for the other coordinates. In DWNA model, the acceleration vector is assumed to be constant during each sampling period.

3.3.2 The State Estimator

Since the measurement equation is a nonlinear function of the target state, a nonlinear tracking filter has to be used. In this study, a first order extended Kalman filter (EKF) is chosen to be the state estimator.

Let $Z_{r1r2\ldots r6}$ be a sextuple sets of measurements consisting of a measurement set from each receiver associated with a track[5]. The EKF measurement update is performed using the batch vector of measurements formed by stacking the nonempty measurement sets given in $Z_{r1r2\ldots r6}$

The Jacobian matrix required to linearize the measurement equations for this batch measurement vector can be found by stacking the Jacobian matrices of measurement equations for each receiver that reports a non-empty measurement set. Let $\hat{X}[t+1|t] = [\hat{x}\ \hat{\dot{x}}\ \hat{y}\ \hat{\dot{y}}\ \hat{z}\ \hat{\dot{z}}]^T$ be the predicted state for a given target at scan $t+1$ and let $R_k = [r_x\ r_y\ r_z]^T$ and $p = [\hat{x}\ \hat{y}\ \hat{z}\ ]^T$ represent the position vectors of receiver k and the predicted target state; then the Jacobian matrix of range and range rate measurement $z_k = [r_k\ \dot{r}_k]^T$ equation is given in Eqs. (26) -9)

$$J = \begin{bmatrix} \frac{dr_k}{dx} & \frac{dr_k}{d\dot{x}} & \frac{dr_k}{dy} & \frac{dr_k}{d\dot{y}} & \frac{dr_k}{dz} & \frac{dr_k}{d\dot{z}} \\ \frac{d\dot{r}_k}{dx} & \frac{d\dot{r}_k}{d\dot{x}} & \frac{d\dot{r}_k}{dy} & \frac{d\dot{r}_k}{d\dot{y}} & \frac{d\dot{r}_k}{dz} & \frac{d\dot{r}_k}{d\dot{z}} \end{bmatrix} \tag{26}$$

$$\frac{dr_k}{d\Psi} = \frac{\hat{\Psi}}{\|p\|} + \frac{\hat{\Psi} - r_\Psi}{\|p - R_k\|} \tag{27}$$

$$\frac{dr_k}{d\dot{\Psi}} = 0 \tag{28}$$

$$\frac{d\dot{r}_k}{d\dot{\Psi}} = \hat{\dot{\Psi}}\left(\frac{1}{\|p\|} - \frac{\hat{\Psi}}{\|p\|^3} + \frac{1}{\|p - R_k\|} - \frac{\hat{\Psi} - r_\Psi}{\|p - R_k\|^3}\right) \tag{29}$$

$$\frac{d\dot{r}_k}{d\dot{\Psi}} = \frac{dr_k}{d\Psi} \tag{30}$$

where $\Psi = \mathrm{x, y\ and\ z}$.

4 At detection probability of 0.9, the requirement will be valid a probability of 0.9842.

5 If not empty, each receiver's measurement set consists of the vector of its measured range and range rate. When no measurement can pass the validation gate test, an empty set is returned by the receiver therefore representing a misdetection

3.3.3 Measurement Association

Let t denote the EKF estimate of a track updated by the sextuple $Z_{r1r2\ldots r6}$, then the association cost of carrying out this update is defined to be the negative of the dimensionless track score function [6-7] which is given in Eq. (31).

$$c_{r1r2\ldots r6} = -\log\frac{\Lambda(Z_{r1r2\ldots r6}|t)}{\Lambda(Z_{r1r2\ldots r6}|\emptyset)} \tag{31}$$

Numerator of the track score function gives the likelihood of the hypothesis where it is considered that every measurement in the set $Z_{r1r2\ldots r6}$ is originated from track *t*. This likelihood function formulized Eq. (32).

$$\Lambda(Z_{r1r2\ldots r6}|t) = \prod_{k=1}^{6}(1-P_d)^{1-u(k)}[P_d p(z_k|t)]^{u(k)} \tag{32}$$

In Eq. (32), z_k represents the measurements from set $Z_{r1r2\ldots r6}$ belonging to receiver k, P_d represents the probability of detection and *u* is an indicator function which returns 1 if z_k is non-empty and zero otherwise. $p(z_k|t)$ can be calculated using the normality of the measurement residual. Denominator of the track score function gives likelihood of the hypothesis where every measurement in $Z_{r1r2\ldots r6}$ is unrelated to the track *t*. Eq. (33) gives this likelihood and Ψ_k symbolizes the volume of the field of view of receiver *k*.

$$\Lambda(Z_{r1r2\ldots r6}|\emptyset) = \prod_{k=1}^{6}[\frac{1}{\Psi_k}]^{u(k)} \tag{33}$$

The goal of the track to measurement association algorithm is to find the track to measurement association with minimum total track score such that:

- Each track is associated with at most one measurement from each receiver.
- Each measurement is associated with at most one track.

For the track initiator module, instead of using the estimate derived by the EKF filter update, the track score is calculated by using the maximum likelihood estimate of the target from the measurement set $Z_{r1r2\ldots r6}$ after which the measurement association for tentative tracks is carried out.

3.3.4 Multidimensional Assignment Solver

It is well known that the cost minimization described above is an NP hard combinatorial optimization problem. In solving this optimization problem, we follow the search algorithm described in the box given below. Although there is no guarantee that the search algorithm will terminate in polynomial time, in our experiments it has been generally observed that the lowest cost association includes lower rank elements from the list of sorted measurement sets, thus this divide and conquer strategy is generally efficient. The time required to solve the multidimensional assignment problem is much lower compared to the time required to do the filtering for all possible measurement sets for each track. Similar findings have been reported in [12].

Multidimensional assignment algorithm	*1- For each track :* *Sort available measurement sets according to their association costs* *2- Associate every track with its lowest cost measurement set and calculate the lower bound for association cost* *3- Check the lower bound association for measurement contentions.* *- if no measurement contention is found return this association,* *- else:* *4- Find the greedy solution and set the return value to the greedy solution* *5- Prune any measurement set with worse association cost than the greedy solution from each track's measurement sets* *6- Divide the region between best possible association cost and the greedy cost to k levels* *7- Starting from the minimum cost level, search for valid measurement set combinations within each level.* *- If a valid measurement set is found, set it as the return value, prune any measurement set with worse association cost from each track's measurement sets and cancel searching lower cost levels.*

3.4 Simulation Results for Multistatic Tracking

In this study we consider a relatively difficult multitarget tracking problem with a multistatic radar system where crossing targets and targets flying in formation are present. Our simulation experiment models a six target scenario inside an observation cell as shown in Figure 9. The first target in the scenario is the control target which is well separated from the other targets. The control target starts its course at an altitude of 9000 meters and moves linearly throughout its course except two maneuvers where it carries out coordinated turns. The first maneuver is a mild 30○ lateral turn and the second maneuver is slightly more aggressive lateral turn accompanied by a climb in altitude. The second and the third targets move linearly at 10000 and 10400 meters respectively. They approach and cross each other with a 400 meter vertical separation. The fourth, fifth and the sixth targets move along the same trajectory with a 400 meter separation at the x axis. In the target scenarios, maneuver accelerations were kept to less than 1 g such that a single tracking filter would be adequate to track targets accurately. To track more agile targets, a multiple model estimator may be used.

Measurements are periodically received at the data processing center at every second. Measurement errors are assumed to be normally distributed with zero mean with standard deviations shown in Table 1. The probability of detection is assumed to be 0.9 for all receivers. Each receiver produces an average of 50 false alarms (Poisson distributed) in every scan. False alarms are created uniformly in between [20000, 60000] meters in range and [-500, +500] meters/second in range rate.

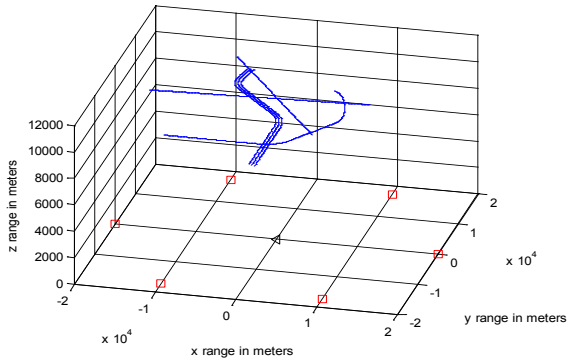

Figure 9: Target trajectories

Table 1. Measurement error standard deviations (range:top, range rate: bottom)

Case I	Case II	Case III
100 m	40 m	40 m
1 m/s	2 m/s	1 m/s

This set up creates a very hard track initiation problem. Although, accurate track initialization was possible, the computational time required to carry out the optimizations to find the maximum likelihood target position estimate for all possible measurement combinations made it infeasible to run the track initiation algorithm at every scan during the whole scenario in our Monte Carlo trials. Thus, for the results given below, the track initiation part of the tracker was turned off and the tracks were initialized with the maximum likelihood estimate for the right measurement combinations. Maximum likelihood estimator's Cramer-Rao lower bound (CRLB) for the initial estimate was used as the initial covariance. The CRLB derivation can be found in [11]. The maximum likelihood estimates were updated with the EKF for 5 additional scans before being fed to the tracker module.

RMS position and velocity error averages of all targets are shown Figs. 9a and 9b. As it can be observed from the figures, the initialization estimate errors decline and arrive at a steady state and increase in the last quarter of the scenario.

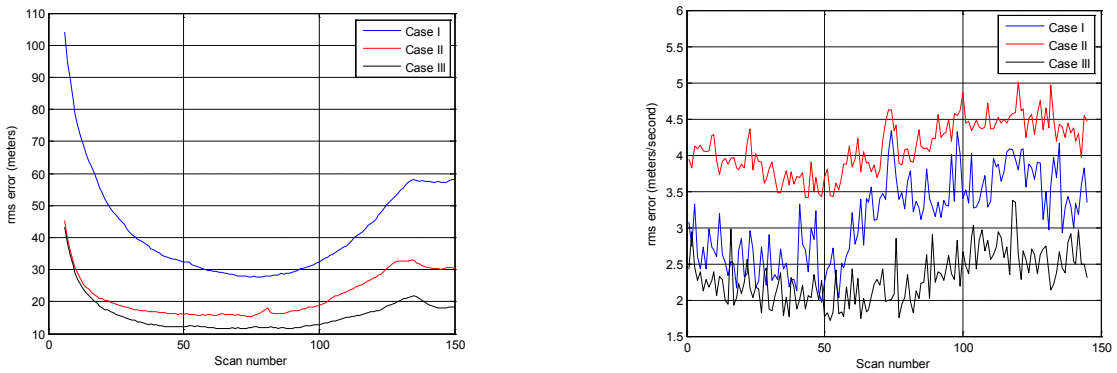

(a) (b)

Figure 9: (a) RMS position error, (b) RMS speed error

The increase in error is caused by target maneuvers. At scan 120, the first target initiates its climb with lateral turn while targets 4-6 carry out coordinated turns. The effects of target maneuvers on the rms position error can be observed in more detail in Figs. 10a and 10b where RMS position error for each target is plotted individually. It can be observed that the jump in error for target 1 is recovered at the end of the maneuver, while the increase in error is permanent for targets 4-6. This is due to false associations and its effect is much more salient for Case III.

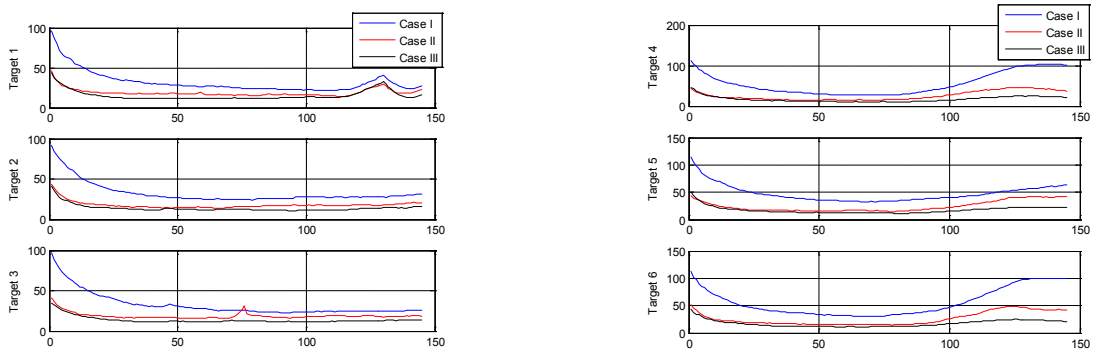

(a) (b)

Figure 10: RMS position error (a) targets 1,2 and 3, (b) targets 4, 5 and 6

The mean rms position and velocity error averages of all targets are tabulated in Table 2. It can be observed that better range measurement leads to better position while better range rate measurement leads to better velocity estimation accuracy. Furthermore, the affect of range rate measurement accuracy is more pronounced than the range measurement accuracy for velocity estimation.

Table 2: Scenario mean rms position and velocity estimate errors

Case I	Case II	Case III
42.46 m	21.86 m	15.77 m
3.13 m/s	4.11 m/s	2.31 m/s

In order to evaluate the association performances, each measurement was tagged with a target number if it were originated by a target or with zero if it were a false alarm. The associated measurements returned by the multidimensional assignment algorithm were then compared to their origins. For the measurements assigned to tracks (misdetections discarded) percentages of measurement origins are tabulated in Tables 3-5. It can be observed from tracks 4-6 that range measurement accuracy is the main contributor for the association success. It shall, however, be kept in mind that, although targets 4-6 are separated by 400 meters in Cartesian space, measured bistatic range difference between two adjacent targets can be as low as 22 meters for certain radars. Apart from causing false associations, this may also lead to unresolved measurements. In this work, we do not consider the case of unresolved measurements.

Table 3: Measurement association percentages for case I

	Track 1 %	Track 2 %	Track 3 %	Track 4 %	Track 5 %	Track 6 %
Track 1	100	0	0	0	0	0
Track 2	0	99.89	0	0.02	0.09	0
Track 3	0	0	100	0	0	0
Track 4	0	0.03	0	83.1	13.81	3.06
Track 5	0	0.09	0	12.99	73.58	13.34
Track 6	0	0.01	0	3.26	13.76	82.97

Table 4: Measurement association percentages for case II

	Track 1 %	Track 2 %	Track 3 %	Track 4 %	Track 5 %	Track 6 %
Track 1	100	0	0	0	0	0
Track 2	0	99.94	0	0	0.05	0
Track 3	0	0	100	0	0	0
Track 4	0	0	0	94.81	4.58	0.61
Track 5	0	0.08	0	4.36	90.73	4.84
Track 6	0	0	0	0.66	5.01	94.32

Table 5: Measurement association percentages for case III

	Track 1 %	Track 2 %	Track 3 %	Track 4 %	Track 5 %	Track 6 %
Track 1	100	0	0	0	0	0
Track 2	0	99.95	0	0	0.05	0
Track 3	0	0	100	0	0	0
Track 4	0	0	0	96.75	2.99	0.26
Track 5	0	0.05	0	2.88	93.77	3.29
Track 6	0	0	0	0.28	3.36	96.37

The average duration of each Monte Carlo run is tabulated in Table 6. Reduction of range error standard deviation decreases measurement contentions for Targets 4-6 which significantly reduces the run time of each Monte Carlo trial.

Table 6: Average Monte Carlo run duration

Case I	Case II	Case III
652 s	171 s	165 s

4.0 USE OF OBSERVED INFORMATION IN MULTISTATIC TRACKING

In this study, the nonlinear state estimation problem in multistatic radar networks has been analyzed. The state estimation in the presence of nonlinear measurements has been addressed through employing particle filtering and fusion of the information gathered from the multiple sources has been handled by using distributed data fusion approach. A study on distributed data fusion via particle filtering has been presented in [13] where posterior distribution of the state has been modeled using *Gaussian Mixture Model* (GMM) and the estimated parameters of the GMM has been shared between the sensors. In [14], the information communicated through the sensors has been summarized using the *Support Vector Machine* (SVM) algorithm and the data fusion has been carried out using consensus filtering. Another study that brings distributed data fusion and particle filtering together was presented in [15] in which a method was proposed overcome the correlated estimation errors arising from the common past information between the two different particle sets. The method is based on converting particle sets into continuous distributions and communicating these distributions between the sensors. Then, common past information is removed by a division operation of two estimates.

In this study, a target tracking algorithm based on particle filtering and distributed data fusion has been proposed. Continuous distribution approximation of the particle set of each sensor has been obtained as in [15] and parameters of these distributions have been communicated between related sensors. However, fusion of the information acquired from the neighboring sensors has been carried out using *Covariance Intersection* (CI) algorithm [16] which provides a consistent way to fuse two pieces of information regardless of the cross-correlation. Unlike [11], in this study, importance distribution of the particle filter exploited at each sensor has been modeled though the posterior *Observed Information Matrix* (OIM) [17]. OIM is described as the negative of the second derivative of the logarithm of the likelihood function and it is a statistical tool used as a surrogate of the *Fisher Information Matrix* (FIM) where FIM is not available. Inverse of the OIM is related to the *Cramer-Rao Bound* (CRB) which defines the theoretical lower bound of the estimation error in terms of the minimum mean square error. Inverse of the posterior OIM has been exploited in modeling the covariance of the importance distribution.

4.1 BACKGROUND

4.1.1 State Estimation

Assume that the target state evolves according to the following discrete time stochastic model,

$$x_k = f_{k-1}(x_{k-1}) + v_{k-1} \tag{34}$$

where $x_k \in R^{n_x}$ is the target state vector, f_{k-1} is known linear/nonlinear function of state and v_{k-1} is process noise which defines any mismodeling effects or unforeseen disturbances in the target motion model. The objective of filtering is to estimate the target state x_k from measurements $z_k \in R^{n_z}$ recursively; where the measurement equation related to the target state is written as follows:

$$z_k = h_k(x_k) + w_k \tag{35}$$

where h_k is a known linear/nonlinear function and w_k is the measurement noise sequence. Under the assumptions given below:

- the noise sequences v_{k-1} and w_k are white, with known probability density functions and mutually independent,
- Distribution of the initial target state $p(x_0)$ is assumed to be known and also to be independent of the noise sequences.

One can calculate the posterior density function of the target state x_k based on measurement sequence $Z_k = \{z_i, i = 1,...,k\}$ up to time k as follows,

$$p(x_k \mid Z_k) = \frac{p(z_k \mid x_k)\, p(x_k \mid Z_{k-1})}{p(z_k \mid Z_{k-1})} \tag{36}$$

$$p(x_k \mid Z_{k-1}) = \int p(x_k \mid x_{k-1})\, p(x_{k-1} \mid Z_{k-1}) dx_{k-1} \tag{37}$$

$$p(z_k \mid Z_{k-1}) = \int p(z_k \mid x_k)\, p(x_k \mid Z_{k-1}) dx \tag{38}$$

where Eqs. (36)-(38) are update equation, prediction equation and normalization constant respectively. Knowledge of the posterior density $p(x_k \mid Z_k)$ enables one to compute an optimal state estimate with respect to any criterion. The recursion given by the equations (36) and (37) is only a conceptual solution to propagation of the posterior density. Analytical solution of these equations can be obtained under some restrictive constraints but it is not discussed here. However, brief discussion about the analytical solutions can be found in [5].

4.1.2 Observed Information Matrix

OIM is a statistical tool used as a surrogate of the FIM when Fisher information is not available and it is described as the negative of second derivative of logarithm of the likelihood function [10]. The likelihood function for bistatic range and range-rate measurements has been constructed under the assumption that measurement noises are mutually independent white Gaussian sequences.

$$\Lambda(r, \dot{r} \mid \theta) = \frac{1}{\sqrt{2\pi}\sigma_m} \exp\left(\frac{-(R_b - r)^2}{2\sigma_m^2}\right) \frac{1}{\sqrt{2\pi}\sigma_{\dot{m}}} \exp\left(\frac{-(\dot{R}_b - \dot{r})^2}{2\sigma_{\dot{m}}^2}\right) \tag{39}$$

In Eq. (39), R_b, $\dot{R}_b$, σ_m^2 and $\sigma_{\dot{m}}^2$ are bistatic range, range-rate, measurement noise variance of bistatic range and measurement noise variance of bistatic range-rate respectively. The *OIM* has been computed using the likelihood function given by Eq. (39) by utilizing Eq. (40). A method for recursive computation of the posterior *OIM* has been given in [10] and this method has been adopted and exploited in this study. The *OIM* given in Eq. (7) defines the contribution of the new measurements to the posterior *OIM* The word "O*IM*" has been used to refer to both *OIM* and the "posterior *OIM"* throughout the text. In Eq. (40), computation of the contribution coming from the new measurements

$$OIM = -\left[\nabla_\theta \nabla_\theta^t \ln(\Lambda(\theta))\right]_{\theta=\hat{\theta}^{MAP}}$$

$$OIM = -\begin{bmatrix} \frac{\partial^2 \ln(\Lambda(\theta))}{\partial x^2} & \cdots & \frac{\partial^2 \ln(\Lambda(\theta))}{\partial x \partial v_z} \\ \vdots & \ddots & \vdots \\ \frac{\partial^2 \ln(\Lambda(\theta))}{\partial v_z \partial x} & \cdots & \frac{\partial^2 \ln(\Lambda(\theta))}{\partial v_z^2} \end{bmatrix}_{\theta=\hat{\theta}^{MAP}} \tag{40}$$

4.1.3 Covariance Intersection Algorithm

Covariance intersection (CI) algorithm was proposed by Julier *et al.* to solve the general data fusion problem where two pieces of information A and B are wanted to be fused to yield the output C [8]. If true statics of A and B are not known and only available information are the estimates of their mean and covariance, consistent estimation of C and its covariance independent of the knowledge of cross correlation between A and B can be obtained by using algorithm proposed in [8]. CI algorithm takes a convex combination of the mean and covariance estimates that are represented information space, i.e. inverse of covariance. Further details of the algorithm have not been given and only the closed form fusion equations of the method have been presented here. However, a brief discussion can be found in [16]. Let P_{AA}, P_{BB} and P_{CC} be the covariances of A, B and C respectively. Consistent estimates of C and P_{CC} are calculated by using Eq.s (41) and (42)

$$P_{CC}^{-1} = wP_{AA}^{-1} + (1-w)P_{BB}^{-1} \tag{41}$$

$$P_{CC}^{-1}C = wP_{AA}^{-1}A + (1-w)P_{BB}^{-1}B \tag{42}$$

where $w \in [0,1]$. In CI algorithm, the fusion weight w is chosen to minimize any measure of covariance P_{CC}. In this study, weights have been computed using Newton-Raphson method in conjunction with the golden section search method for solving constraint optimization problem given below.

$$\begin{aligned} &w = \arg\min\left\{\det\left(P_{CC}^{-1}\right)\right\} \\ &w \in [0,1] \end{aligned} \tag{42}$$

4.1.4 Sampling Importance Resampling Particle Filter

In this study, a particle filter based target tracking algorithm has been implemented. It is assumed that each receiver has its own tracker and all the receivers share their tracker outputs with each other. Each tracker is assumed to be capable of estimating the target position and velocity in 3D Cartesian space and the tracker output consists of estimated target state and its covariance. The fusion mechanism brings all the tracker outputs together and fuses them by using Covariance Intersection (CI) algorithm. Sampling Importance Resampling (SIR) particle filter algorithm has been implemented at each receiver site. This algorithm can be easily obtained by modifying Sequential Importance Sampling (SIS) algorithm [4]. The algorithm is derived from the SIS algorithm by choosing importance density to be the transitional density $p(x_k \mid x_{k-1})$ and performing the resampling step at every time update. In the SIR particle filter, there are two simple assumptions: *i)* State dynamics and measurements functions are known, *ii)* It is possible to sample realizations from the prior and transitional distributions. If these two assumptions are satisfied, SIR particle filter is initiated by drawing samples from the prior distribution and time updates of the filter is recursively implemented as follows:

- Draw samples at time k $x_k^i \sim p\left(x_k \mid x_{k-1}^i\right)$
- Calculates weights $w_k^i = p\left(z_k \mid x_k^i\right)$
- Normalize weights

$$\tilde{w}_k^i = \frac{w_k^i}{\sum_{i=1}^{N} w_k^i}$$

- Calculate state estimation and its covariance

$$\hat{x}_k = \sum_{i=1}^{N} \tilde{w}_k^i x_k^i, \qquad \hat{P}_k = \sum_{i=1}^{N} \tilde{w}_k^i \left(\hat{x}_k - x_k^i\right)\left(\hat{x}_k - x_k^i\right)^T$$

- Resample the samples generated at time k with respect to the weights.

4.2 Combining SIR Particle Filter, CI Algorithm and OIM

In this study, the state estimation and its covariance have been computed through the SIR particle filter algorithm at each receiver site and the outcomes have been sent to the fusion center to obtain the final target state and covariance estimations. It should be noted that there is no separate dedicated fusion center and each receiver node acts as a fusion center. The most important part of the SIR particle filter is the resampling step where degeneracy of the particles is prevented by resampling particles with respect to the weights. In the classical SIR particle filter, particles which have low weights are replaced with the particles which have larger weights. However, while working with the bistatic range and range-rate measurements, one must have at least three measurements obtained from different receiver sites to be able to estimate the target state in 3D Cartesian space. That is, the SIR particle filter deployed at each receiver site does not have adequate information to estimate the target state and the particle weights used at resampling step are inadequate to choose the right particles from the particle set which are going to be used at the next recursion of the filter. It is obvious that particle resampling in the presence of lack of information would result in divergence of the filter. One way of overcoming this problem is to utilize the fused state estimation at the resampling step. The fused state estimation can be taken into account by using the fused posterior distribution, which summarizes all the information up to time k. If one could draw samples from the fused posterior distribution and move the samples forward in time with respect to Eq. (34), the new particle set would represent the transitional prior given in the first step of the SIR algorithm.

Using this approach at the resampling step is equivalent to forgetting all the particles contributing to computation of the fused posterior, which is valid under the assumption that state is a Markov process and the posterior distribution includes all the information up to time k. The drawback of using the fused posterior distribution arises from employing CI algorithm as a fusion method. CI algorithm combines the information (mean and covariance) coming from the different sources and obtains a fused covariance covering the intersection region of the covariances which participates in the fusion process. This approach overestimates the true fused covariance where it lies in the region of the intersection of the covariances to be fused. Illustration of the one-sigma ellipses of two covariances, namely P1, P2, their convex combination with respect to various weights and the true fused covariance are shown in Fig. 11. As it can be seen in Fig. 1, convex combination of the two covariances leads to a larger covariance than the true fused covariance. This result represents the basic idea of the CI algorithm. However, if one wants to draw samples by using the posterior distribution with this covariance, the particles are always going to be spread in a volume greater than the required.

Therefore, we propose a new importance distribution based on the posterior Observed Information Matrix for the resampling. The obvious choice in this particular fusion application would be to utilize the posterior OIM computed around the fused estimation and employing the available measurements from the sensors. Inverse of this information would be highly related to the Posterior Cramer Rao Bound (PCRB) and simulation based analysis confirms this relation. By definition the PCRB defines the minimum achievable variance for an estimator which means that estimators which have the variance equal to the PCRB would have the minimum uncertainty volume.

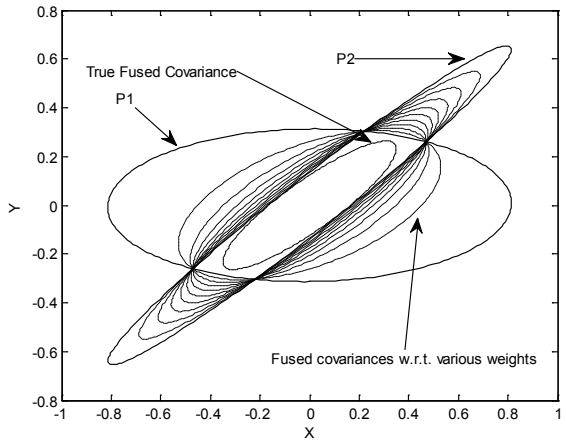

Figure 11: One-sigma covariance ellipses obtained by fusing P_1 and P_2

This means, if we had an efficient state estimator, covariance of the posterior distribution would be the PCRB and utilizing the OIM^{-1} would give an opportunity to get samples from the desired posterior distribution. The goal of exploiting posterior distribution with this covariance, i.e., OIM^{-1}, at the resampling step is to draw samples from a smaller volume than that could be achieved fused covariance based posterior distribution is used. Thus, more samples would be scattered around the true target state.

A viable question at this point would be `why use OIM instead of PCRB?`, as PCRB is a better way to represent the `*information*`. The very basic answer to this question is that *PCRB* is computed around the true target state, which is only available in simulations, in other words, the PCRB is a statistical tool that could only be computed theoretically thus, cannot be used directly in real world applications. On the other hand, the inverse of *OIM* is computed around the estimated state and the latest measurement and it can be used as a surrogate of the PCRB.

One cycle of the target tracking algorithm based on utilization of CI, particle filter and *OIM* has been given below. The algorithm has been divided into two branches, namely *A* and *B*, which share their outputs with each other to construct the final state estimation. In step *A*, the SIR particle filter that uses the particle set drawn from the importance distribution computes the sensor level state estimation and its covariance. These quantities are shared with the neighboring sensors. In step *B*, sensor level state estimations and their covariances acquired from the other sensors are combined via CI algorithm. Output of CI algorithm is the final state estimation $\hat{x}_k^{fused}$ and its covariance $\hat{P}_k^{fused}$. At the end of this step, the OIM is evaluated around the final state estimation.

One cycle of the algorithm

A) At each sensor

1. *Generate N particles from the importance distribution computed using* OIM^{-1} *at the last update and set all weights to 1/N*

   $N\left(\hat{x}_k^{fused}, OIM^{-1}\right)$

2. *Move particles in time w.r.t. Eq. 1*
3. *Calculate weights*
4. *Normalize weights*
5. *Estimate target's state and covariance*

   $$\hat{x}_k^j = \sum_{i=1}^{N} w_{k,j}^i x_{k,j}^i,\ i = 1,...,N,\ j = 1,...,P$$

   $$\hat{P}_k^j = \sum_{i=1}^{N} w_{k,j}^i \left(\hat{x}_k^j - x_{k,j}^i\right)\left(\hat{x}_k^j - x_{k,j}^i\right)^T$$

6. *Send state estimation and its covariance, sensor measurements to the neighboring sensors.*

B) At fusion stage

1. *Sort the estimates in descending order w.r.t. the determinant of inverse of their covariances.*
2. *Begin fusion with the first two sorted estimates.*
3. *Calculate fusion weights to minimize the determinant of fused covariance.*
4. *Calculate fused state estimate, covariance*
5. *Return to step 3 until all sensor estimates fused with previous fusion result.*
6. *Set final fusion results as the estimate of target state and covariance.*

Calculate OIM around the final estimate and share with other sensors

4.3 SIMULATION RESULTS

In this study, results of information analysis in the passive radar network given in [11] have been used for modeling a multistatic radar network. A network consisting of a single transmitter and six receivers with the capability of measuring bistatic range and range rate has been modeled. The analysis carried out here is independent of target detection processes, i.e., target is assumed to have been detected and a track has been initialized. The multistatic radar network is assumed to output bistatic range and range rate measurements that are generated by each transmitter-receiver pair and those measurements are corrupted by additive white Gaussian noise with known mean and covariance. In the analysis, plane earth model is used and coverage area of the multistatic radar network is kept limited in both X and Y axes in the interval of (-40km, 40km). Transmitter of the network is assumed to be at the origin of the 3D Cartesian space and receivers are located to form a circle around the transmitter. Circle radius is chosen to be 30km and angular separation of two successive receivers is assumed be 60°. All the receivers and the transmitter are assumed to be located at zero altitude. A target trajectory has been created to test the performance of the algorithms. Target starts its motion at (-40km, 20km, 10km) point in 3D Cartesian coordinate system with the velocity vector (100, 0, 0) m/sec. Target moves according to nearly constant velocity model for 800sec. and flies over the multistatic radar network. Transmitter and receiver locations with the assumed target trajectory has been shown in Fig. 1b., where the transmitter location is indicated with a star and receiver locations are marked with dots. The solid line seen in the figure is the target trajectory and the beginning of the trajectory has been marked with a cross. Measurements obtained from each transmitter-receiver pair for 3D target state have been given as defined by Eqs. (15) and (16), where additive error terms ε_r and $\varepsilon_{\dot{r}}$ are assumed to be independent white Gaussian processes with zero mean and variances of $\sigma_R^2 = 10000\,m^2$ and $\sigma_{\dot{R}}^2 = 1(m/\sec)^2$ respectively. Some assumptions that pertaining to the simulations are given below:

- There is only one target in surveillance region and it is detected at every measurement time.
- Target state vector at time k is given by $\bar{x}_k = (x_k, \dot{x}_k, y_k, \dot{y}_k, z_k, \dot{z}_k)^T$ and target moves according to the nearly constant velocity model [3],
- Track has been initialized.
- Prior target distribution is Gaussian with the mean equal to the initial value of true target state and covariance $P_0 = diag\left(10^4\, 15^2\, 10^4\, 15^2\, 10^4\, 15^2\right)$.
- *N=2000* particles are used at each sensor of the network for the CI based data fusion.

Performance of the data fusion algorithms presented in this study has been compared via simulations where the root mean square (RMS) error has been used as a performance metric. Two different importance distributions have been modeled by using *i)* inverse of the posterior OIM and *ii)* covariance of the state estimation obtained via fusion process and target tracking performance of the algorithm under the different importance distributions has been investigated via 100 Monte Carlo simulations. Position RMS errors in X, Y and Z axes have been given in Figures 12a, 12b and 12c respectively. Simulation results has revealed that using the importance distribution based on final posterior distribution leads to better RMS error performance in comparison with the case where the importance distribution of the particle filters constructed by the inverse of posterior *OIM*. However, average of RMS error differences of two algorithms in X, Y and Z axes is only 2.88m, 1.44m and 4.85 m, respectively. As it can be seen from the figures, the larger RMS error difference occurs at the initial and last phase of the target tracking where the target is moving outside of the receiver circle shown in Fig. 1b. If a comparison only in terms of RMS errors is made, then the target tracking algorithm exploiting *OIM* would be considered unsuccessful in contrast to the algorithm utilizing posterior distribution.

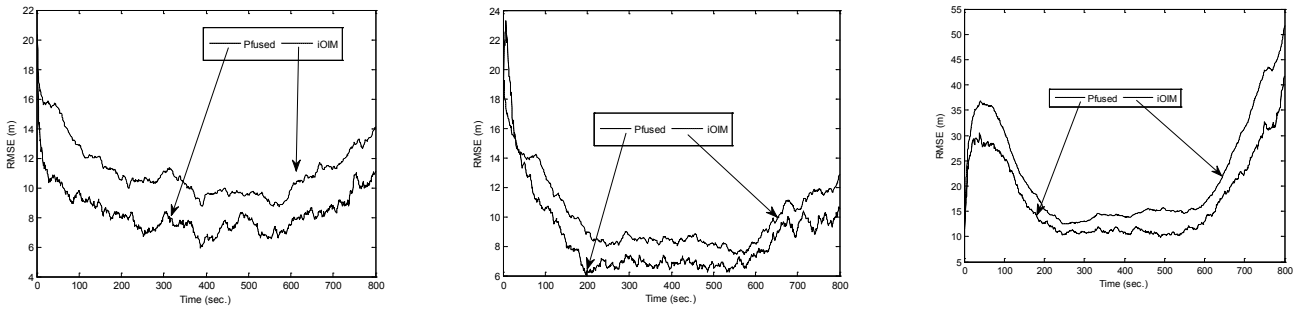

(a) (b) (c)

Figure 12: RMS error on (a) X axis, (b) Y axis, (c) Z axis

However, uncertainty associated with the estimation is as important as the accuracy of the estimation. Thus, estimation covariances have been analyzed via simulations and the results have been given in Figures 4a, 4b and 4c. In Fig. 4a, variation of square root of the *X* component of the covariances, i.e., standard deviations, has been given as an average of the Monte Carlo simulations. Simulation results have shown that, exploiting *OIM* has yielded about 1.5 times smaller standard deviation on average along the *X* axis. Supporting results have also been obtained for the Y and Z axes which given in Figures 4b and 4c.

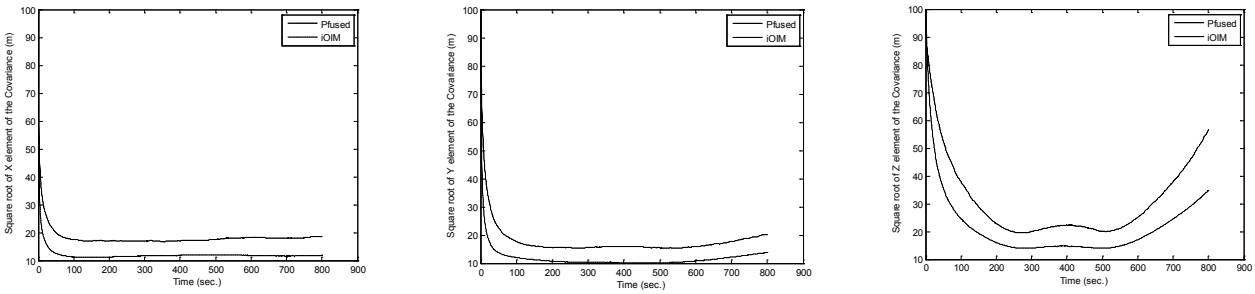

(a) (b) (c)

Figure 13: Square root of the (a) X component, (b) Y component, (c) Z component of the covariance

Physical meaning of the estimation covariance is that it is the volume of the uncertainty associated with the estimation and it corresponds to a hyper-ellipsoid. The volume of this hyper-ellipsoid has an important role when target tracking is carried out in the presence of measurement origin uncertainty, i.e., target tracking in multiple target and/or clutter environment. In the presence of measurement origin uncertainty, one should be able to associate measurements with the targets with relative ease. This process is known as the data association in the literature [3]. The smaller volume reduces the probability of presence of measurements which are not related to target of interest. Hence, small uncertainty volume associated with a target is a desired situation in the data association process. Variation of the square root of determinant of the covariances which are related to volume has been given in Fig. 14. Simulation results have revealed that, around 5 times smaller uncertainty volume can be achieved by utilizing *OIM* compared to the utilization of the posterior distribution.

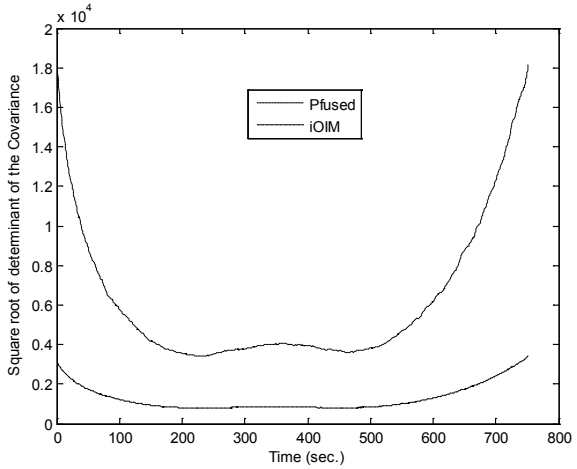

Figure 14: Square root of the determinant of the covariance.

Normalized Estimation Error Square (NEES) has also been computed for the both cases via simulations and the variation of the NEES has been given in Fig. 15. In Fig. 15, the region seen between lines passing through the points 5.33 and 6.69 on Y axis is 0.99 probability region that NEES is expected to be in it. However, computed NEESs are below the lower bound of that region which means, the true covariance associated with the state estimate has been overestimated in both cases, i.e., estimation covariances achieved for both cases are larger than the covariance which is expected to be realized for the obtained estimation error levels. However, the larger NEES values depicted in Fig. 15 corresponds to the covariance more related to the true estimation errors and the larger NEES values are obtained by exploiting *OIM* in the importance distribution of the particle filter.

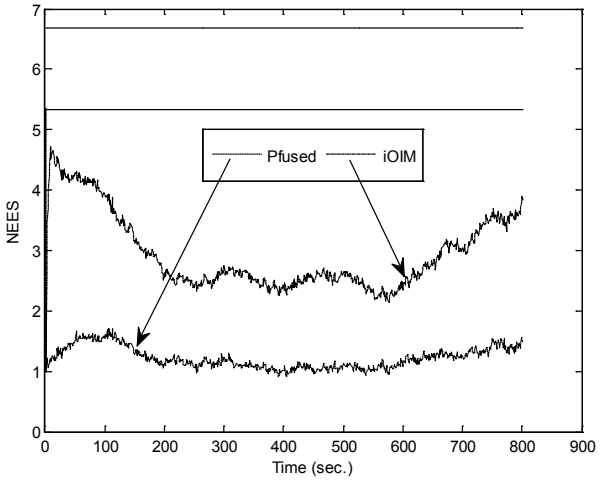

Figure 15: Variation of the NEES.

Simulation results have shown that exploiting *OIM* has led to larger RMS errors in all axes. However, it has been observed that the performance degradation in terms of RSM error is at acceptable levels. Major contribution of exploiting *OIM* has been observed in estimation of the state covariance. Simulation results have revealed that smaller covariance estimation compared to the case in which posterior distribution is used, can be obtained by exploiting *OIM* for given scenario. That means, smaller uncertainty volume can be

achieved, that is a desired situation in data association problems. Data association problem is encountered in multi target tracking where origin of the measurements is uncertain. In this case, one should determine the measurement which is originated form the target of interest and this process is called as *Data Association*. Since the smaller estimation covariance exploited in data association leads to more accurate measurement to track association [3], utilization of the OIM in estimation process would improve overall performance of the tracking system.

5.0 REFERENCES

[1] N. J. Willis, and H. D. Griffiths Advances in Bistatic Radar, SCITECH Publishing, Raleigh NC-USA, 2007

[2] H. D. Griffiths, "Bistatic and Multistatic Radar", IEE Military Radar Seminar, Shrivenham, UK, 2004.

[3] Bar-Shalom, Y., Li, X. R., Kirubarajan, T. Estimation with Application to Tracking and Navigation, Wiley – Interscience Publication, 2001.

[4] Julier S., Uhlmann J., and Hugh F. D. W. A New Method for the Nonlinear Transformation of Means and Covariances in Filters and Estimators, IEEE Transactions on Automatic Control, Vol. 45, No. 3, p. 477-482, 2000.

[5] Ristic B., Arulampalam S., Gordon N. Beyond the Kalman Filter, Artech House 2004.

[6] A. Farina, "Tracking function in bistatic and multistatic radar systems", IEE Proceedings F Communications, Radar and Signal Processing, Volume 133, Issue 7, pp. 630-637, 1986.

[7] M. Tobias , and A. Lanterman, "Probability hypothesis density-based multitarget tracking with bistatic range and Doppler observations," Sonar and Navigation, IEE Proceedings, vol. 152, no. 3, pp. 195-205, June 2005.

[8] M. Daun, and W. Koch, "Multistatic target tracking for non-cooperative illumination by DAB/DVB-T" IEEE Radar Conference, Rome 2008, pp.1 - 6.

[9] S. Deb, M. Yeddanapudi, K.R. Pattipati, and Y. Bar-Shalom, "A generalized S-D assignment algorithm for multisensor-multitarget state estimation." IEEE Transactions on Aerospace and Electronic Systems, Vol 33 pp. 523-538, April 1997.

[10] T. Sathyan, A. Sinha, and T. Kirubarajan, "Passive geolocation and tracking of an unknown number of emitters", IEEE Transactions on Aerospace and Electronic Systems, Volume 42, Issue 2, pp. 740-750, April 2006.

[11] Soysal G., Bozdogan A. O., Efe, M. Information Analysis in Passive Radar Networks for Target Tracking, 12th International Conference on Information Fusion, p. 1115 - 1122, July 2009, Seattle.

[12] A. Sinha and T. Kirubarajan, "A randomized heuristic approach for multidimensional association in target tracking", Proc. SPIE edited by E Drummond, Volume 5428, pp. 202-210, 2004.

[13] Dongbing, G. Distributed Particle Filter for Target Tracking, IEEE International Conference on Robotics and Automation, p. 3856-3861, April 2007, Rome.

[14] Liu ,H. Q., So, H. C., Chan, F. K. W., and Liu, K. W. K. Distributed Particle Filter for Target Tracking in Sensor Networks, Progress In Electromagnetics Research C, Vol. 11, p.171-182, 2009.

[15] Lee-Ling O., Tim B., Hugh D. W., and Ben U. Decentralized Particle Filtering for Multiple Target Tracking in Wireless Sensor Networks, 11th International Conference on Information Fusion, p. 1-8, July 2008, Cologne.

[16] Julier S. and Uhlmann J. K. Hand Book of Multisensor Data Fusion, Chapter 12, CRC Press LLC, 2001.

[17] Streit R. L. Observed Information Matrices for Multistatic Target and Sensor Field Tracking, Oceans, p. 1-6, June 2007, Aberdeen.

6.0 APPENDIX

$$-E\left[\frac{\partial^2\varphi}{\partial x^2}\right]=\frac{1}{\sigma_m^2}\left(\frac{x-x_r}{R_r}+\frac{x-x_t}{R_t}\right)^2+\frac{1}{\sigma_{\dot m}^2}\left(\frac{vx}{R_r}+\frac{vx}{R_t}-\frac{(x-x_r)\dot R_r}{R_r^2}-\frac{(x-x_t)\dot R_t}{R_t^2}\right)^2$$

$$-E\left[\frac{\partial^2\varphi}{\partial y^2}\right]=\frac{1}{\sigma_m^2}\left(\frac{y-y_r}{R_r}+\frac{y-y_t}{R_t}\right)^2+\frac{1}{\sigma_{\dot m}^2}\left(\frac{vy}{R_r}+\frac{vy}{R_t}-\frac{(y-y_r)\dot R_r}{R_r^2}-\frac{(y-y_t)\dot R_t}{R_t^2}\right)^2$$

$$-E\left[\frac{\partial^2\varphi}{\partial z^2}\right]=\frac{1}{\sigma_m^2}\left(\frac{z-z_r}{R_r}+\frac{z-z_t}{R_t}\right)^2+\frac{1}{\sigma_{\dot m}^2}\left(\frac{vz}{R_r}+\frac{vz}{R_t}-\frac{(z-z_r)\dot R_r}{R_r^2}-\frac{(z-z_t)\dot R_t}{R_t^2}\right)^2$$

$$-E\left[\frac{\partial^2\varphi}{\partial x\partial vx}\right]=\frac{1}{\sigma_{\dot m}^2}\left(\frac{x-x_r}{R_r}+\frac{x-x_t}{R_t}\right)x\left(\frac{vx}{R_r}+\frac{vx}{R_t}-\frac{(x-x_r)\dot R_r}{R_r^2}-\frac{(x-x_t)\dot R_t}{R_t^2}\right)$$

$$-E\left[\frac{\partial^2\varphi}{\partial x\partial vy}\right]=\frac{1}{\sigma_{\dot m}^2}\left(\frac{y-y_r}{R_r}+\frac{y-y_t}{R_t}\right)x\left(\frac{vx}{R_r}+\frac{vx}{R_t}-\frac{(x-x_r)\dot R_r}{R_r^2}-\frac{(x-x_t)\dot R_t}{R_t^2}\right)$$

$$-E\left[\frac{\partial^2\varphi}{\partial x\partial vz}\right]=\frac{1}{\sigma_{\dot m}^2}\left(\frac{z-z_r}{R_r}+\frac{z-z_t}{R_t}\right)x\left(\frac{vx}{R_r}+\frac{vx}{R_t}-\frac{(x-x_r)\dot R_r}{R_r^2}-\frac{(x-x_t)\dot R_t}{R_t^2}\right)$$

$$-E\left[\frac{\partial^2\varphi}{\partial y\partial vz}\right]=\frac{1}{\sigma_{\dot m}^2}\left(\frac{z-z_r}{R_r}+\frac{z-z_t}{R_t}\right)x\left(\frac{vy}{R_r}+\frac{vy}{R_t}-\frac{(y-y_r)\dot R_r}{R_r^2}-\frac{(y-y_t)\dot R_t}{R_t^2}\right)$$

$$-E\left[\frac{\partial^2\varphi}{\partial y\partial vx}\right]=\frac{1}{\sigma_{\dot m}^2}\left(\frac{x-x_r}{R_r}+\frac{x-x_t}{R_t}\right)x\left(\frac{vy}{R_r}+\frac{vy}{R_t}-\frac{(y-y_r)\dot R_r}{R_r^2}-\frac{(y-y_t)\dot R_t}{R_t^2}\right)$$

$$-E\left[\frac{\partial^2\varphi}{\partial y\partial vy}\right]=\frac{1}{\sigma_{\dot m}^2}\left(\frac{y-y_r}{R_r}+\frac{y-y_t}{R_t}\right)x\left(\frac{vy}{R_r}+\frac{vy}{R_t}-\frac{(y-y_r)\dot R_r}{R_r^2}-\frac{(y-y_t)\dot R_t}{R_t^2}\right)$$

$$-E\left[\frac{\partial^2\varphi}{\partial z\partial vy}\right]=\frac{1}{\sigma_{\dot m}^2}\left(\frac{y-y_r}{R_r}+\frac{y-y_t}{R_t}\right)\left(\frac{vz}{R_r}+\frac{vz}{R_t}-\frac{(z-z_r)\dot R_r}{R_r^2}-\frac{(z-z_t)\dot R_t}{R_t^2}\right)$$

$$-E\left[\frac{\partial^2\varphi}{\partial z\partial vx}\right]=\frac{1}{\sigma_{\dot m}^2}\left(\frac{x-x_r}{R_r}+\frac{x-x_t}{R_t}\right)x\left(\frac{vz}{R_r}+\frac{vz}{R_t}-\frac{(z-z_r)\dot R_r}{R_r^2}-\frac{(z-z_t)\dot R_t}{R_t^2}\right)$$

$$-E\left[\frac{\partial^2\varphi}{\partial z\partial vz}\right]=\frac{1}{\sigma_{\dot m}^2}\left(\frac{z-z_r}{R_r}+\frac{z-z_t}{R_t}\right)x\left(\frac{vz}{R_r}+\frac{vz}{R_t}-\frac{(z-z_r)\dot R_r}{R_r^2}-\frac{(z-z_t)\dot R_t}{R_t^2}\right)$$

$$-E\left[\frac{\partial^2\varphi}{\partial x\partial y}\right]=\frac{1}{\sigma_m^2}\left(\frac{x-x_r}{R_r}+\frac{x-x_t}{R_t}\right)\left(\frac{y-y_r}{R_r}+\frac{y-y_t}{R_t}\right)+\frac{1}{\sigma_{\dot m}^2}\left(\frac{vx}{R_r}+\frac{vx}{R_t}-\frac{(x-x_r)\dot R_r}{R_r^2}-\frac{(x-x_t)\dot R_t}{R_t^2}\right)x$$
$$\left(\frac{vy}{R_r}+\frac{vy}{R_t}-\frac{(y-y_r)\dot R_r}{R_r^2}-\frac{(y-y_t)\dot R_t}{R_t^2}\right)$$

$$-E\left[\frac{\partial^2\varphi}{\partial x\partial z}\right]=\frac{1}{\sigma_m^2}\left(\frac{x-x_r}{R_r}+\frac{x-x_t}{R_t}\right)\left(\frac{z-z_r}{R_r}+\frac{z-z_t}{R_t}\right)+\frac{1}{\sigma_{\dot{m}}^2}\left(\frac{vx}{R_r}+\frac{vx}{R_t}-\frac{(x-x_r)\dot{R}_r}{R_r^2}-\frac{(x-x_t)\dot{R}_t}{R_t^2}\right)x$$
$$\left(\frac{vz}{R_r}+\frac{vz}{R_t}-\frac{(z-z_r)\dot{R}_r}{R_r^2}-\frac{(z-z_t)\dot{R}_t}{R_t^2}\right)$$

$$-E\left[\frac{\partial^2\varphi}{\partial y\partial z}\right]=\frac{1}{\sigma_m^2}\left(\frac{y-y_r}{R_r}+\frac{y-y_t}{R_t}\right)\left(\frac{z-z_r}{R_r}+\frac{z-z_t}{R_t}\right)+\frac{1}{\sigma_{\dot{m}}^2}\left(\frac{vy}{R_r}+\frac{vy}{R_t}-\frac{(y-y_r)\dot{R}_r}{R_r^2}-\frac{(y-y_t)\dot{R}_t}{R_t^2}\right)x$$
$$\left(\frac{vz}{R_r}+\frac{vz}{R_t}-\frac{(z-z_r)\dot{R}_r}{R_r^2}-\frac{(z-z_t)\dot{R}_t}{R_t^2}\right)$$

$$-E\left[\frac{\partial^2\varphi}{\partial vx^2}\right]=\frac{1}{\sigma_{\dot{m}}^2}\left(\frac{x-x_r}{R_r}+\frac{x-x_t}{R_t}\right)^2$$

$$-E\left[\frac{\partial^2\varphi}{\partial vy^2}\right]=\frac{1}{\sigma_{\dot{m}}^2}\left(\frac{y-y_r}{R_r}+\frac{y-y_t}{R_t}\right)^2$$

$$-E\left[\frac{\partial^2\varphi}{\partial vz^2}\right]=\frac{1}{\sigma_{\dot{m}}^2}\left(\frac{z-z_r}{R_r}+\frac{z-z_t}{R_t}\right)^2$$

$$-E\left[\frac{\partial^2\varphi}{\partial vx\partial vy}\right]=\frac{1}{\sigma_{\dot{m}}^2}\left(\frac{x-x_r}{R_r}+\frac{x-x_t}{R_t}\right)\left(\frac{y-y_r}{R_r}+\frac{y-y_t}{R_t}\right)$$

$$-E\left[\frac{\partial^2\varphi}{\partial vx\partial vz}\right]=\frac{1}{\sigma_{\dot{m}}^2}\left(\frac{x-x_r}{R_r}+\frac{x-x_t}{R_t}\right)\left(\frac{z-z_r}{R_r}+\frac{z-z_t}{R_t}\right)$$

$$-E\left[\frac{\partial^2\varphi}{\partial vy\partial vz}\right]=\frac{1}{\sigma_{\dot{m}}^2}\left(\frac{y-y_r}{R_r}+\frac{y-y_t}{R_t}\right)\left(\frac{z-z_r}{R_r}+\frac{z-z_t}{R_t}\right)$$